Biophysical Journal
Biophysical Letter

Biophysical Society

Force Spectroscopy with 9-μs Resolution and Sub-pN Stability by Tailoring AFM Cantilever Geometry

Devin T. Edwards,[1] Jaevyn K. Faulk,[1] Marc-André LeBlanc,[2] and Thomas T. Perkins[1,3,*]
[1]JILA, National Institute of Standards and Technology and University of Colorado, Boulder, Colorado; [2]Department of Chemistry and Biochemistry and [3]Department of Molecular, Cellular, and Developmental Biology, University of Colorado, Boulder, Colorado

ABSTRACT Atomic force microscopy (AFM)-based single-molecule force spectroscopy (SMFS) is a powerful yet accessible means to characterize the unfolding/refolding dynamics of individual molecules and resolve closely spaced, transiently occupied folding intermediates. On a modern commercial AFM, these applications and others are now limited by the mechanical properties of the cantilever. Specifically, AFM-based SMFS data quality is degraded by a commercial cantilever's limited combination of temporal resolution, force precision, and force stability. Recently, we modified commercial cantilevers with a focused ion beam to optimize their properties for SMFS. Here, we extend this capability by modifying a 40 $\times$ 18 μm^2 cantilever into one terminated with a gold-coated, 4 $\times$ 4 μm^2 reflective region connected to an uncoated 2-μm-wide central shaft. This "Warhammer" geometry achieved 8.5-μs resolution coupled with improved force precision and sub-pN stability over 100 s when measured on a commercial AFM. We highlighted this cantilever's biological utility by first resolving a calmodulin unfolding intermediate previously undetected by AFM and then measuring the stabilization of calmodulin by myosin light chain kinase at dramatically higher unfolding velocities than in previous AFM studies. More generally, enhancing data quality via an improved combination of time resolution, force precision, and force stability will broadly benefit biological applications of AFM.

Single-molecule force spectroscopy (SMFS) provides valuable insights into diverse biophysical systems (1). One particularly exciting application is studying the unfolding and refolding of nucleic acid structures (2) and proteins (3,4). Detecting closely spaced and/or transiently occupied intermediate states yields insights into a molecule's folding pathway (5–9). Such studies require a technically challenging triumvirate of experimental capabilities: temporal resolution, force precision, and force stability. Temporal resolution and force precision are needed to distinguish closely spaced and briefly occupied states. Force stability enables equilibrium assays, where individual molecules repeatedly unfold and refold (2) and thereby also enables reconstruction of a one-dimensional free-energy landscape along the stretching axis (10). Dual-beam optical traps have emerged as the SMFS modality of choice for such studies (6–8,10) due to their combination of force stability and precision. For instance, studies of calmodulin with an optical trap resolved additional folding intermediates (7) that were previously undetected by highly stable, custom atomic force microscopy (AFM) (11).

Historically, AFMs have had poor force precision and stability in comparison to custom-built optical traps (1). However, commercial AFMs are much more user accessible. SMFS on a modern AFM is now limited by the mechanical properties of commercial cantilevers rather than the rigidity of the AFM frame (12–14). For example, we achieved sub-pN stability over 100 s by removing the gold coating from long, soft cantilevers (L = 100 μm; $k \approx$ 7 pN/nm) (12). Yet these cantilevers still suffered from relatively poor force precision and time resolution (450 ms) in comparison to the best optical trapping results (15).

A high-speed AFM using ultrashort cantilevers (L = 9 μm) (16), on the other hand, has exceeded the time resolution of advanced optical traps (15) (0.7 versus 6–10 μs, respectively). However, this benefit comes at the expense of force precision due to underdamped motion (quality factor (Q) $>$ 0.5) and stability due to low-frequency (low-f) noise (14). Recently, we optimized ultrashort cantilevers for SMFS by modifying them with a focused ion beam (FIB), achieving 1-μs resolution and improved force precision (14). Yet these cantilevers had only moderate stability, achieving sub-pN performance over ~1–3 s. Further,

Submitted August 29, 2017, and accepted for publication October 11, 2017.
*Correspondence: tperkins@jila.colorado.edu
Editor: Keir Neuman.
https://doi.org/10.1016/j.bpj.2017.10.023

detecting such modified, ultrashort cantilevers required retrofitting our commercial AFM with a home-built detection system (14). Thus, there is an exciting opportunity in AFM-based SMFS to combine excellent time resolution and extended force stability with the ease of use provided by an unmodified commercial AFM.

Here, we extend our earlier efforts in modifying cantilevers with an FIB (13,14) to achieve 8.5-μs resolution coupled with sub-pN stability over 100 s on an unmodified commercial AFM. We demonstrated the utility of this, to our knowledge, new cantilever geometry by unfolding a single protein domain embedded in a polyprotein (Fig. 1 *A*), and thereby resolved a calmodulin unfolding intermediate previously undetected by AFM (11). We also measured calmodulin stabilization by myosin light chain kinase (MLCK) at much higher unfolding velocities than in earlier AFM studies (11).

Our new "Warhammer" cantilever is best understood if we briefly review the process and benefits of FIB-modifying cantilevers. To achieve detection with our commercial AFM (Cypher ES; Asylum Research, Goleta, CA), we started with a cantilever of intermediate length, a BioLever Mini ($L = 40$ μm; $k \approx 100$ pN/nm; Olympus) (Fig. 1 *B*). Relative to the oft-used BioLever Long ($L = 100$ μm; $k \approx 7$ pN/nm; Olympus), this shorter and stiffer cantilever offered improved short-term force precision due to its lower hydrodynamic drag (β) (17) and improved time resolution ($\tau \approx k/\beta$ in the overdamped limit [$Q < 0.5$]). However, these benefits come at the expense of force stability due to low-f noise that increases with k. Our original FIB-modifying process yielded a soft yet short cantilever ($L = 40$ μm; $k \approx 7$ pN/nm) (Fig. 1 *C*) (13). In that work, we simultaneously reduced k and β by removing a rectangular region at the base of the cantilever and thinning the remaining supporting beams. We then removed the majority of the cantilever's gold coating to improve force stability, and retained high reflectivity by preserving a small gold patch at the end of the cantilever. For brevity, we refer to these cantilevers as a "Mod Mini." In our original work (13), they exhibited a good response time (76 μs) by SMFS standards coupled with sub-pN force stability over five decades of time (0.001–100 s).

Using this basic FIB-modification process, we hypothesized that reducing β via reduced surface area at the end of the cantilever would further improve performance. Such reduction could be accommodated while still efficiently detecting the resulting cantilever by using the small spot-size (9×3 μm^2) detection module available for our commercial AFM. In particular, we tested two new cantilever geometries, referred to as "Long-cut Mini" and Warhammer (Fig. 1, *D* and *E*). Although the Long-cut Mini was an extension of our original Mod Mini (Fig. 1 *C*) (13), the Warhammer used a small (4×4 μm^2) yet highly reflective region supported by a central uncoated shaft. We modified all cantilevers to have a ~10-fold

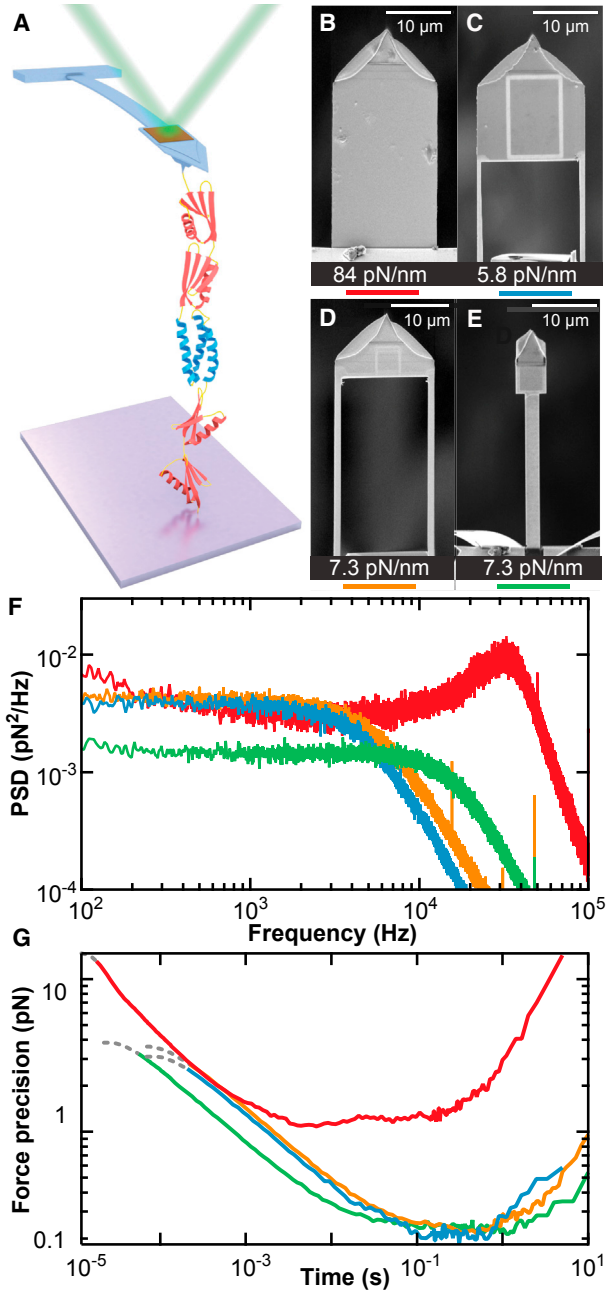

FIGURE 1 Improved performance of modified AFM cantilevers. (*A*) Schematic of the assay showing a polyprotein consisting of four domains of NuG2 (*red*) and one domain of α_3D (*blue*) being unfolded with a Warhammer cantilever. (*B–E*) Images of cantilevers prior to gold removal: an unmodified BioLever Mini (*B*), a standard Mod Mini (*C*), a Long-cut Mod Mini (*D*), and a Warhammer (*E*). The cantilever's spring constant is noted below each image. (*F*) Comparison of the force PSD for each cantilever using the color code denoted in (*B*)–(*E*). (*G*) Force precision over a given averaging time, technically the Allan deviation (17). At the very shortest times, the motion of the cantilever becomes correlated, distorting the force precision calculation. This region of the curve is de-emphasized using a dashed line.

reduction in k. We did not investigate very soft cantilevers ($k < 4$ pN/nm), which tend to irreversibly fold when immersed in liquid.

To compare our set of four cantilever geometries, we measured their thermal motion in liquid positioned 50 nm over the surface and thereby deduced their force power spectral density (PSD) (Fig. 1 *F*) and force precision (Fig. 1 *G*). Specifically, we computed the mean force precision over a given averaging time, technically the Allan deviation (18). Importantly, these metrics reflect performance in typical SMFS assays because they account for the increased β when a cantilever is positioned near a surface.

Analysis of the PSD reveals several benefits arising from FIB modification. First, a standard BioLever Mini remained resonant even near the surface ($Q = 1.9$), as illustrated by the peak in its PSD at ~32 kHz (Fig. 1 *F*, *red*). Yet, standard SMFS theory assumes the force probe is overdamped ($Q < 0.5$) (19). All three modified cantilevers exhibited PSDs with no peak. Unexpectedly, the Long-cut Mini exhibited a PSD essentially identical to a standard Mod Mini (Fig. 1 *F*, *orange* versus *blue*) despite removing an extra 30% of the cantilever's planar surface area. In contrast, the Warhammer geometry had a ~3-fold higher characteristic frequency (f_c) and better force precision in the thermally limited regime (flat portion of the PSD). Hence, both time resolution and force precision improved despite constant k. Our results, therefore, suggest that a single supporting shaft has substantially reduced β relative to two widely spaced supports. Finite-element modeling may provide for further enhancements.

Computing force precision as a function of averaging time highlights that averaging Brownian motion over short timescales improved data quality (Fig. 1 *G*). Over longer timescales, force precision was degraded due to low-f noise. For these four cantilevers, the Warhammer had the best stability, with similar performance by the other two modified cantilevers. The Warhammer also exhibited the best short-term force precision due to its lower β. More quantitatively, the Warhammer had ~40% less force noise than a Mod Mini in the thermally limited regime (0.2–10 ms).

We next compared the performance of the three modified cantilevers (Fig. 2 *A*) when applied to the unfolding of a polyprotein, a widely used assay (Fig. 1 *A*). To do so, we used a polyprotein containing a single copy of α_3D centered within four repeats of NuG2 (20). NuG2 is a fast-folding variant of GB1 (21) that has been well studied by AFM (22), and acts as an internal standard to assure individual polyproteins were stretched. α_3D is a computationally designed, three-helix bundle (23), and is the most mechanically labile protein probed to date by AFM-based SMFS (20). For improved data quality, we site-specifically anchored one end to a polyethylene glycol-coated cover slip via a copper-free click chemistry, and the other end to a polyethylene glycol-coated AFM tip via a streptavidin-biotin linkage. This scheme enabled a strong but reversible coupling to the AFM tip (20).

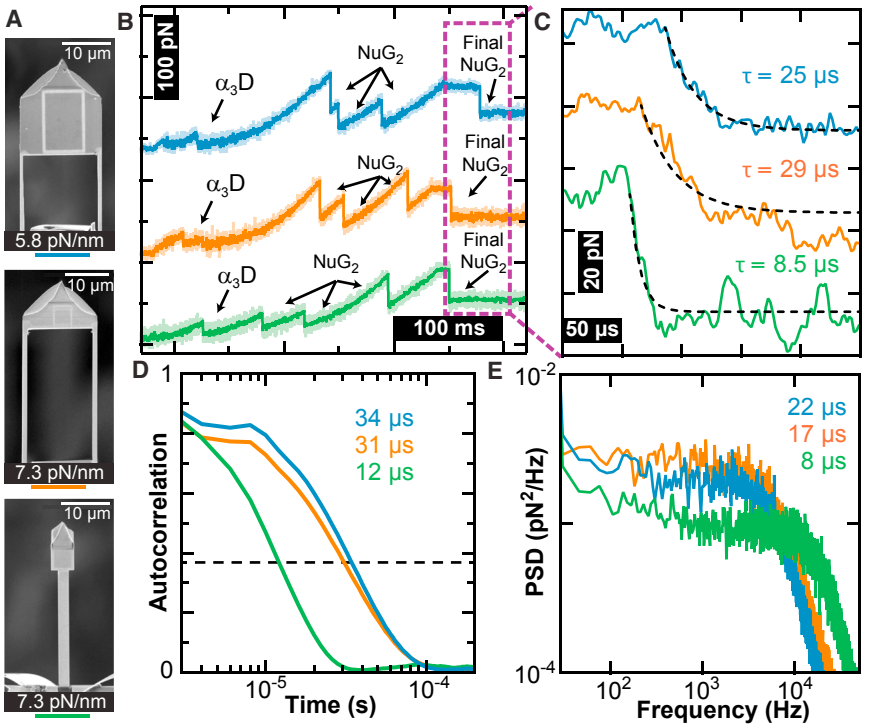

FIGURE 2 **Temporal resolution of different cantilever geometries. (*A*) Scanning electron microscopy images of the modified cantilevers. (*B*) Force-versus-time traces show unfolding of the (NuG2)$_2$-α_3D-(NuG2)$_2$ construct. In this assay, the construct was stretched until the α_3D and three NuG2 domains unfolded. The stage was further retracted until the polyprotein was held at ~80 pN. The stage retraction was then stopped and the last folded NuG2 domain unfolded. Data smoothed to 2 kHz. (*C*) High-bandwidth force-versus-time traces from (*B*) showing the unfolding of the fourth NuG2 domain at $v = 0$ nm/s. Time constants determined from exponential fits. Data acquired at 500 kHz. (*D*) Autocorrelation of the cantilever motion after the final NuG2 domain unfolded but was still attached to the polyprotein. Time constants shown were determined from the 1/e point of the autocorrelation (*dashed line*). (*E*) Force PSDs of the 500-kHz data after unfolding of the final NuG2 domain. Time constants estimated from $\tau \approx Q/(\pi f_c)$ based on the characteristic frequency, f_c.**

To directly measure the cantilever response time during a SMFS assay, we used a stretching protocol in which we initially unfolded α_3D and the first three NuG2 domains at $v = 400$ nm/s, and then stopped retraction at ~80 pN (Fig. 2 *B*) to measure the resulting force decay after the rupture of the final NuG2 domain (Fig. 2 *C*). This mechanical response to a step change in force was well described by a single exponential. Comparison among the modified cantilevers showed that the Warhammer had a decay time of 8.5 μs, a 3-fold improvement over the Long-cut Mini and the Mod Mini (29 and 25 μs, respectively). Additionally, all three cantilevers clearly resolved the low-force unfolding of α_3D.

Although this force decay is our preferred metric, the cantilever response time is also encoded in the Brownian motion of the cantilever. In particular, we computed two alternative metrics by analyzing the cantilever's thermal motion when pulling on the fully unfolded polyprotein, because the taut polyprotein contributes added stiffness to the full system during a SMFS assay. In the first alternative, we estimated the cantilever response time from the 1/e point in the cantilever's autocorrelation curve (Fig. 2 *D*), yielding a characteristic time similar to our preferred metric. The second metric was based on analysis of force PSDs (Fig. 2 *E*), similar to Fig. 1 *D*, but when pulling on the polyprotein. Based on a traditional AFM analysis (16), the response time was estimated using $\tau \approx Q/(\pi f_c)$. Although this estimate is accurate in the underdamped limit ($Q >> 1$), the resulting response times were nevertheless similar to the other metrics. Finally, we note that careful inspection of Fig. 2 *C* leads to an apparent anomaly: the Warhammer has larger force fluctuations and hence larger force noise than the other two modified cantilevers. In actuality, the Warhammer has better force precision (Fig. 1, *G* and *F*); this discrepancy arises from the temporal filtering by the slower responding cantilevers given the depicted 500-kHz data (Fig. 2 *C*). When the data from all three cantilevers were filtered to 5 kHz (Fig. S1), the Warhammer exhibited better force precision (1.7 pN) than either the Mod Mini (2.4 pN) or the Long-cut Mini (2.6 pN).

To demonstrate the Warhammer's improved performance in AFM-based SMFS, we revisited a pioneering AFM study that resolved the unfolding and refolding of calmodulin (11). To review, this prior work used a custom AFM to pull at very low velocities ($v = 1$ nm/s) and thereby revealed two unfolding steps: the N-terminal and C-terminal domains, each of which is composed of two EF-hand motifs. However, a subsequent study using a dual-beam optical trap revealed an additional intermediate in which one of the EF-hand motifs in the C-terminal domain unfolds (7). With the Warhammer, we now observed this additional unfolding intermediate, and did so at a comparatively high stretching velocity (100 nm/s) relative to the original AFM work (1 nm/s) (Fig. 3, *A* and *B*). For clarity, we color coded the three unfolding states, fully folded (*blue*), partial unfolding of the C-terminal EF hand (*green*), full unfolding of the C-terminal domain (*orange*), and the fully unfolded calmodulin (*purple*). As expected, the total change in contour length (53.0 nm) agreed with the previously measured value (52.2 nm) (7).

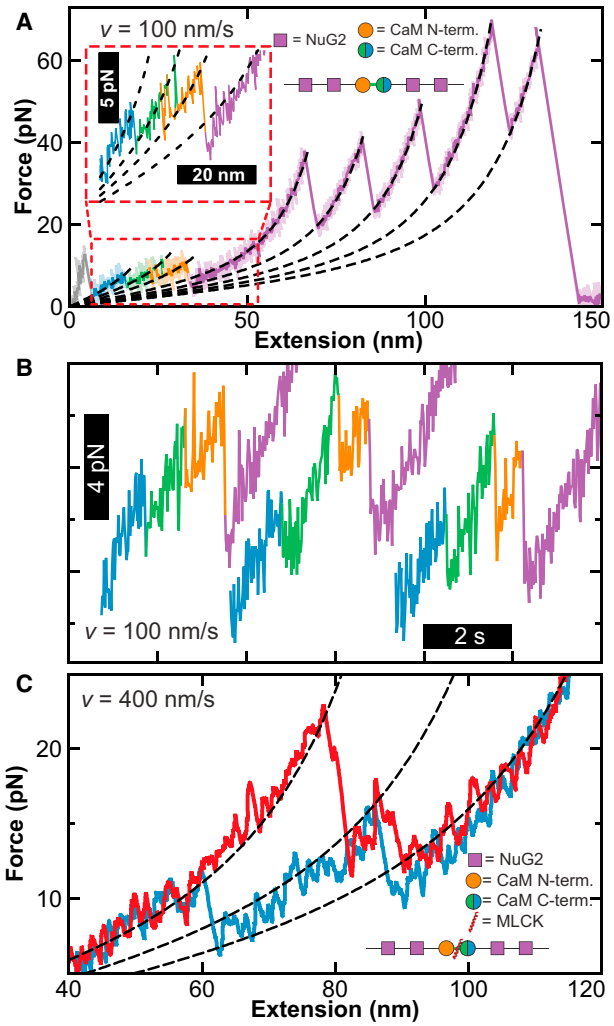

FIGURE 3 Improved AFM-based SMFS studies of calmodulin unfolding when using a Warhammer cantilever. (*A*) Force-extension curves show the unfolding of a polyprotein containing calmodulin and four repeats of NuG2 at $v = 100$ nm/s. Trace color coding indicates fully folded calmodulin (*blue*), partial unfolding of the N-terminal domain (*green*), followed by the full unfolding of the C- and N-terminal domains (*orange* and *purple*, respectively). The unfolding of the NuG2 domains at higher force is also color coded purple. Dashed lines represent worm-like chain fits. (*Inset*) Calmodulin unfolding at low force. (*B*) Three force-versus-time traces at $v = 100$ nm/s highlight three-step unfolding of calmodulin. (*C*) Force-extension curves comparing the unfolding of calmodulin bound and unbound to MLCK at $v = 400$ nm/s (*red* and *blue*, respectively). Dark traces filtered to 250 Hz.

We next recapitulated the mechanical stabilization of calmodulin when bound to one of its target ligands, MLCK (11). In that earlier study, MLCK stabilized the N-terminal

domain. When we added MLCK to the buffer, we also clearly observed MLCK-induced stabilization (Fig. 3 *C*, *red* versus *blue*) despite pulling at much higher velocity (400 versus 1 nm/s). Thus, the Warhammer provides for significantly enhanced signal/noise ratio and rapid characterization of low-force unfolding events by AFM standards (1,11)

From a practical point of view, we emphasize that FIB-modified cantilevers were straightforward to fabricate and were reusable. Until recently (13), our laboratory had no prior expertise with an FIB. After initial training in FIB operation, fabrication of the Warhammer geometry was not technically challenging, but rather a modification of a previously published, step-by-step protocol (24). The change in geometry, on the other hand, was the key to improved performance. Fabrication remained efficient; we produced 2–3 cantilevers/h. Unlike FIB-modified, ultrashort cantilevers (14), we detected the Warhammer when using the standard small spot-size module of our commercial AFM with no loss in precision over all measured frequencies (Fig. S2 *A*). That said, we preferred to use a home-built module that featured a 3-μm diameter circular spot (14) because it reduced an optical interference artifact (Fig. S2 *B*). Finally, Warhammer cantilevers were robust and reusable. After functionalization (20), a Warhammer could be reused over multiple days and refunctionalized after plasma cleaning. Handling or bending of the cantilever during plasma cleaning was typically the limiting factor.

In summary, Warhammer cantilevers offer an excellent combination of 8.5-μs resolution coupled with sub-pN force stability over 100 s. We expect this combination to enable equilibrium folding studies of proteins and nucleic acid structures over long periods on a commercial AFM. The advances in data quality demonstrated here for SMFS are immediately applicable to a wide range of biological AFM applications, including rapid nanomechanical mapping of live cells (25).

SUPPORTING MATERIAL

Supporting Materials and Methods and seven figures are available at http://www.biophysj.org/biophysj/supplemental/S0006-3495(17)31141-4.

AUTHOR CONTRIBUTIONS

T.T.P. designed the research. M.-A.L. purified labeled polyprotein constructs. D.T.E. and J.K.F. fabricated the cantilevers. D.T.E. acquired the data, and D.T.E. and T.T.P. analyzed the data and wrote the manuscript.

ACKNOWLEDGMENTS

We thank M. Sousa for scientific discussions.

This work was supported by a National Institutes of Health Molecular Biophysics Training grant awarded to M.-A.L. (T32 GM-065103), by the National Science Foundation (grants DBI-1353987, MCB-1716033, and Phy-1734006), and by the National Institute of Standards and Technology (NIST). Mention of commercial products is for information only; it does not imply NIST's recommendation or endorsement. T.T.P. is a staff member of NIST's Quantum Physics Division.

SUPPORTING CITATIONS

References (26–29) appear in the Supporting Material.

REFERENCES

1. Neuman, K. C., and A. Nagy. 2008. Single-molecule force spectroscopy: optical tweezers, magnetic tweezers and atomic force microscopy. *Nat. Methods.* 5:491–505.
2. Liphardt, J., B. Onoa, …, C. Bustamante. 2001. Reversible unfolding of single RNA molecules by mechanical force. *Science.* 292:733–737.
3. Rief, M., M. Gautel, …, H. E. Gaub. 1997. Reversible unfolding of individual titin immunoglobulin domains by AFM. *Science.* 276:1109–1112.
4. Cecconi, C., E. A. Shank, …, S. Marqusee. 2005. Direct observation of the three-state folding of a single protein molecule. *Science.* 309:2057–2060.
5. Onoa, B., S. Dumont, …, C. Bustamante. 2003. Identifying kinetic barriers to mechanical unfolding of the T. thermophila ribozyme. *Science.* 299:1892–1895.
6. Greenleaf, W. J., K. L. Frieda, …, S. M. Block. 2008. Direct observation of hierarchical folding in single riboswitch aptamers. *Science.* 319:630–633.
7. Stigler, J., F. Ziegler, …, M. Rief. 2011. The complex folding network of single calmodulin molecules. *Science.* 334:512–516.
8. Yu, H., X. Liu, …, M. T. Woodside. 2012. Direct observation of multiple misfolding pathways in a single prion protein molecule. *Proc. Natl. Acad. Sci. USA.* 109:5283–5288.
9. Yu, H., M. G. Siewny, …, T. T. Perkins. 2017. Hidden dynamics in the unfolding of individual bacteriorhodopsin proteins. *Science.* 355:945–950.
10. Woodside, M. T., P. C. Anthony, …, S. M. Block. 2006. Direct measurement of the full, sequence-dependent folding landscape of a nucleic acid. *Science.* 314:1001–1004.
11. Junker, J. P., F. Ziegler, and M. Rief. 2009. Ligand-dependent equilibrium fluctuations of single calmodulin molecules. *Science.* 323:633–637.
12. Churnside, A. B., R. M. Sullan, …, T. T. Perkins. 2012. Routine and timely sub-picoNewton force stability and precision for biological applications of atomic force microscopy. *Nano Lett.* 12:3557–3561.
13. Bull, M. S., R. M. Sullan, …, T. T. Perkins. 2014. Improved single molecule force spectroscopy using micromachined cantilevers. *ACS Nano.* 8:4984–4995.
14. Edwards, D. T., J. K. Faulk, …, T. T. Perkins. 2015. Optimizing 1-μs-resolution single-molecule force spectroscopy on a commercial atomic force microscope. *Nano Lett.* 15:7091–7098.
15. Neupane, K., D. A. Foster, …, M. T. Woodside. 2016. Direct observation of transition paths during the folding of proteins and nucleic acids. *Science.* 352:239–242.
16. Rico, F., L. Gonzalez, …, S. Scheuring. 2013. High-speed force spectroscopy unfolds titin at the velocity of molecular dynamics simulations. *Science.* 342:741–743.
17. Viani, M. B., T. E. Schaffer, …, P. K. Hansma. 1999. Small cantilevers for force spectroscopy of single molecules. *J. Appl. Phys.* 86:2258–2262.
18. Sullivan, D. B., D. W. Allan, …, E. L. Walls. 1990. Characterization of Clocks and Oscillators. U.S. Government Printing Office, Washington.
19. Evans, E., and K. Ritchie. 1999. Strength of a weak bond connecting flexible polymer chains. *Biophys. J.* 76:2439–2447.
20. Walder, R., M.-A. LeBlanc, …, T. T. Perkins. 2017. Rapid characterization of a mechanically labile α-helical protein enabled by efficient site-specific bioconjugation. *J. Am. Chem. Soc.* 139:9867–9875.

21. Nauli, S., B. Kuhlman, and D. Baker. 2001. Computer-based redesign of a protein folding pathway. *Nat. Struct. Biol.* 8:602–605.

22. Cao, Y., R. Kuske, and H. Li. 2008. Direct observation of markovian behavior of the mechanical unfolding of individual proteins. *Biophys. J.* 95:782–788.

23. Zhu, Y., D. O. Alonso, …, F. Gai. 2003. Ultrafast folding of alpha3D: a de novo designed three-helix bundle protein. *Proc. Natl. Acad. Sci. USA.* 100:15486–15491.

24. Faulk, J. K., D. T. Edwards, …, T. T. Perkins. 2017. Improved force spectroscopy using focused-ion-beam-modified cantilevers. *Methods Enzymol.* 582:321–351.

25. Alsteens, D., V. Dupres, …, Y. F. Dufrêne. 2012. High-resolution imaging of chemical and biological sites on living cells using peak force tapping atomic force microscopy. *Langmuir.* 28:16738–16744.

26. Proksch, R., T. E. Schaffer, …, M. B. Viani. 2004. Finite optical spot size and position corrections in thermal spring constant calibration. *Nanotechnology.* 15:1344–1350.

27. Cao, Y., M. M. Balamurali, …, H. Li. 2007. A functional single-molecule binding assay via force spectroscopy. *Proc. Natl. Acad. Sci. USA.* 104:15677–15681.

28. He, C., C. Hu, …, H. Li. 2015. Direct observation of the reversible two-state unfolding and refolding of an alpha/beta protein by single-molecule atomic force microscopy. *Angew. Chem. Int. Ed. Engl.* 54:9921–9925.

29. Bouchiat, C., M. D. Wang, …, V. Croquette. 1999. Estimating the persistence length of a worm-like chain molecule from force-extension measurements. *Biophys. J.* 76:409–413.

Biophysical Journal, Volume *113*

Supplemental Information

Force Spectroscopy with 9-μs Resolution and Sub-pN Stability by Tailoring AFM Cantilever Geometry

Devin T. Edwards, Jaevyn K. Faulk, Marc-André LeBlanc, and Thomas T. Perkins

Supporting Information

Force Spectroscopy with 9-μs Resolution and Sub-pN Stability by Tailoring AFM Cantilever Geometry

Devin T. Edwards,[1] Jaevyn K. Faulk,[1] Marc-André LeBlanc,[2] and Thomas T. Perkins[1,3,*]

[1]JILA, National Institute of Standards and Technology and University of Colorado, Boulder, Colorado 80309, USA; [2]Department of Chemistry and Biochemistry, [3]Department of Molecular, Cellular, and Developmental Biology, University of Colorado, Boulder, Colorado 80309, USA;

MATERIALS & METHODS:

SUPPORTING FIGURES & TABLES:

MATERIALS & METHODS:

FIB MODIFICATION OF CANTILEVERS

Cantilever selection: To accurately compare cantilever performance due to difference in modifications, we wanted to start with cantilevers that exhibited the same mechanical properties. To do so, we selected ~15 cantilevers from two commercial packs for pre-calibration. The stiffness of each cantilever was then determined in air, as described in detail below. We next recorded the thermal motion of the cantilever in liquid after positioning it 50 nm from the surface. From this data, we calculated the force power spectral density (PSD) for each lever. We next selected for modification a subset of the measured cantilevers that exhibited similar stiffnesses (k), characteristic frequencies (f_c), and quality factors (Q). The k and PSD for each of the 3 modified cantilevers used in the main manuscript are shown in Fig. S3. While in this present work we focused on comparing the performance of these three cantilevers along with an unmodified cantilever, we have made tens to hundreds of Warhammers and Mod Minis, respectively.

FIB modification: Each of the three modified cantilevers followed a similar FIB protocol, with small differences noted below. In general, we used a previously published step-by-step protocol for fabricating a Modified BioLever Mini (*i.e.*, "Mod Mini") (1). Briefly, as diagrammed in Fig. S4 A, we first used a defocused ion beam to etch a rectangular trench of 8×12 μm^2 at the end of the cantilever by milling only through the gold and chromium capping layer. Next, we used a tightly focused ion beam to cut three sides of a rectangle through the cantilever. The two cuts along the length of the cantilever extend slightly onto the supporting chip. This step left two ~1 μm-wide supporting "legs." In the next cut, we cut along the base of the cantilever connecting the two cuts along the long axis of the cantilever. This cut caused a rectangular "flap" to fold up. Next, to further reduce k and eliminate FIB-induced bending of the cantilever, we simultaneously thinned both the legs. We then coated the rectangular patch defined by the shallow trench at the end of the cantilever with tetraethyl orthosilicate (TEOS) using electron-beam-induced deposition. This process resulted in a transparent capping layer that protected the coated region during a subsequent pair of wet chemical etches that sequentially removed the gold and underlying chromium layers. The trench, not used in our original FIB-modification protocol (2), helped ensure that the TEOS layer firmly adhered to the silicon nitride cantilever and thereby prevented undercutting of the gold and chromium during the wet chemical etch.

To make a Long-cut Mini (Fig. S4 B), we used a nearly identical protocol. The only distinction is that the TEOS trench was 4×4 μm^2, allowing the rectangular flap to extend to ~5 μm from the end of the cantilever.

To make a Warhammer cantilever (Fig. S4 C), we started with the same size TEOS frame as the long-cut Mini. However, instead of cutting out the rectangular frame, we instead cut around either side of the TEOS trench and all the way back to the cantilever chip, leaving only a single 2-μm-wide central supporting shaft. We then cut these outer flaps along the base of the cantilever,

which caused them to bend upwards and out of the way. The rest of the modification process then preceded as with the other cantilevers. We note that these flaps either remained attached to the chip after immersion in liquid or detached. Only very rarely did the flaps interfere with the use of a cantilever. We also note that we found that the back side of the cantilever directly above the tip did not contribute to the reflected laser light (*i.e.*, sum signal on the QPD) when it was gold coated. Hence, in our final design, we did not leave this area gold-coated.

AFM INSTRUMENTATION

AFM: We collected our data on a Cypher ES AFM (Asylum Research) and used its temperature controlled, closed fluidic cell to maintain 25 °C, except as noted. To detect the cantilevers, we used two detection modules available from Asylum Research that had different spot sizes: a standard-spot-size laser diode (30×10 μm^2) and a small-spot-size super-luminescent diode (SLD) (9×3 μm^2). The commercial small-spot-size module detected modified cantilevers with no loss in force precision across the full measured bandwidth (Fig. S2 A) as compared to a previously described, custom-built detection system that featured an even smaller spot size (3-μm-diameter) (3). For completeness, we note that this custom unit now also utilizes an SLD instead of a laser diode, since it led to a decrease in an optical-interference artifact when detecting a Warhammer cantilever (Fig. S2 B). Such an artifact is common when detecting an ultrashort cantilever (L = 9 μm) (4). We measured the spot profile of the commercial small-spot-size module (Fig. S2 C) and that of our circular-small-spot module (Fig. S2 D). To do so, we placed a 1-μm diameter iris on top of a photodiode in our commercial AFM. Then, without a cantilever installed, we focused the detection laser onto the surface and used the AFM to scan the iris through the laser beam while recording the photodiode voltage.

To reduce optical-interference artifacts for users of the commercial small spot size module, we developed a variant of the Warhammer—an extended Warhammer (Fig. S2 E)—that used a slightly narrower but longer reflective region (2.7×7.4 μm^2) than our standard one (4 ×4 μm^2) (Fig. S2 F) that better matched the spot size of the commercial unit. As expected, this variant significantly reduced the optical-interference artifact (Fig. S2 B, orange vs. purple, respectively) at minimal reduction in f_c (16 vs 19 kHz, respectively) (Fig. S2 A). Finally, we emphasize that even much larger interference fringes do not interfere with biological interpretation of AFM-based SMFS and, hence users can take full advantage of the performance gains afforded by a standard Warhammer and then computationally subtract out the interference artifact in post-processing of the data. Indeed, we have previously computationally subtracted out much larger interference artifacts of ~400 pN peak-to-peak that arose when applying FIB-modified ultrashort cantilevers (L = 9 μm) (5).

Cantilever characterization: To determine k, we measured the cantilever's stiffness in air since the Q of the cantilever was higher. We first determined detection sensitivity (nm/V) by pressing the cantilever into hard contact with a mica or cleaned glass surface. A surface indentation of at

least 500 pN was used to achieve a linear force-vs-position curve, and the sensitivity was determined from a fit to the linear portion of this indentation curve. We then retracted the cantilever until it was >1 μm from the surface. Next, we measured the cantilever's thermal motion at high bandwidth (typically 2 MHz) and fit the first harmonic of the resulting PSD (6). This process was repeated at least 3 times in different spots around the surface. The resulting values of k were averaged to assign a k to a cantilever. Subsequently, all measurements in fluid utilized this k as a known constant and analyzed the PSD in liquid to determine the sensitivity, in analogy with a calibration protocol developed for ultrashort cantilevers (4). In general, if thermal calibration is performed in liquid, the resulting probe stiffness agrees to within ±15% of the stiffness determined in air.

To provide insight into a cantilever's performance in single-molecule assays, we next calculated two metrics. To do so, we let the cantilever settle for ~2 h after mounting and immersion in liquid. We next positioned the cantilever 50 nm above the surface to account for increased hydrodynamic drag near a surface (*i.e.*, squeezed film damping in the language of the AFM instrumentation community) and then recorded the thermal motion of the cantilever for ~100 s at 500 kHz. For these measurements, the X-, Y-, and Z- feedback loops on the AFM were engaged to hold the AFM chip at a constant location above the surface. From these records, we computed force PSDs. To reduce noise in the spectrum, we divided the traces into ~20 shorter traces and then averaged the PSDs from these short traces. The same 100 s trace was used to calculate the force precision, strictly the Allan deviation: $\sigma_F(T) = \sqrt{\frac{1}{2}\langle(\bar{F}_{i+1} - \bar{F}_i)^2\rangle_T}$, where F_i is the mean value of the data over the i^{th} time interval of T duration (7). One of the virtues of the Allan deviation is it shows on what timescale increased averaging of Brownian motion over longer periods for improved force precision becomes limited by instrumental noise.

Improved sub-pN force stability by increased settling time: Prior work from our lab showed that we could achieve sub-pN performance 30 min after mounting the cantilever in liquid when measuring an Olympus BioLever Long ($k \approx 7$ pN/nm) that had had its metallic coating removed (8). With the Warhammer geometry, we observed sub-pN force precision, as measured by the Allan deviation, at 100 s typically 1 h after mounting. While longer than for an uncoated BioLever Long, it is still a rather minimal settling time by AFM-based SMFS standards. That said, not every cantilever exhibited this level of stability. However, standard Mod. Mini cantilevers with similar k consistently achieved a sub-pN Allan deviation at 100 s under similar conditions (2). To account for this variation, we measure the Allan deviation ~1 h after mounting to determine the suitability of a particular cantilever when needing the highest level of force stability.

Ongoing work is trying to determine the origin of these differences between individual cantilevers. Somewhat unexpectedly, we observed force stability varied with the precise vertical position of the detector beam focus relative to the cantilever when measuring the same Warhammer cantilever (Fig. S5 A). The detailed mechanism leading to this result remains under investigation.

On usability, we note that slight defocusing of the cantilever reduces the optical-interference artifact but degrades force stability. Given our prior success in computationally subtracting out even large optical-interference artifacts (5), we recommend positioning the beam waist of the detector beam in the plane of the cantilever (though this recommendation may vary for different AFMs).

To investigate if extended settling times could further improve force stability, we measured the force precision as a function of averaging time at 4 h and 14 h after mounting in liquid. In particular, we had achieved 0.5 pN stability at 100 s when letting the cantilever settle for 14 h, about a two-fold improvement over what we measured at 4 h (Fig. S5 B). We note that one advantage of our commercially available, temperature-regulated sample holder is that this level of stability can be achieved while holding the biological sample at 4 °C during the overnight settling period and then warming it up for use the following morning. Hence, this level of stability should be available even for temperature-sensitive samples. Finally, we note that these results suggest that force instability was more closely associated with immersion of the cantilever through the air-water interface, rather than the temperature history of the cantilever.

SINGLE-MOLECULE ASSAY

Coverslip and AFM tip functionalization: To improve the quality of our AFM data, we site-specifically stretched our polyprotein construct between a polyethylene glycol (PEG)-coated glass coverslip and AFM tip (9). In this scheme, we labeled the biomolecule of interest using a biotin moiety at one end and dibenzocyclooctyne (DBCO), a copper-free click reagent, at the other end. This scheme allowed us to couple the labeled polyprotein to an azide-functionalized coverslip and then stretch it using a streptavidin-coated AFM tip. We functionalized coverslips with a short silane-PEG-azide reagent (PG2-AZSL-600, Nanocs Inc), as previously detailed (9). To make streptavidin-coated AFM tips, we first functionalized the silicon-nitride tips using a silane-PEG-maleimide reagent (PG2-MLSL-600, Nanocs Inc). After rinsing, we then reacted the cantilevers with thiol-derivatized streptavidin (SAVT, Protein Mods LLC). Protein-coated coverslips and AFM tips were stored in PBS [10 mM phosphate buffer (pH 7.4), 140 mM NaCl, 3 mM KCl] at 4 °C prior to use and could be reused over multiple days.

Polyprotein construct: For our site-specific coupling scheme, we used a labeled polyprotein construct containing four repeats of NuG2, as recently described (9). Briefly, NuG2 served as a marker protein to assure only individual molecules were analyzed. NuG2 is a fast-folding variant of GB1 (10) and well-characterized by AFM (11,12). We embedded the protein of interest—α_3D or calmodulin—into the middle of this construct. Because none of these proteins contained an internal cysteine, we labeled the polyprotein via two cysteines positioned near the N- and C-terminals of the polyprotein (as opposed to converting them to aldehydes using an enzymatic reaction) (9). To functionalize with both DBCO and biotin, we reacted the polyprotein with a 10-fold molar excess of both sulfo-maleimide-PEG$_4$-DBCO (Click Chemistry Tools) and maleimide-

biotin (Sigma) overnight at room temperature. While only a fraction of the constructs will be orthogonally labeled with biotin and DBCO, only these constructs were efficiently stretched between an azide-functionalized surface and a streptavidin-coated AFM tip.

After purifying away the unreacted reagents, this labeled polyprotein was deposited onto azide-functionalized glass coverslips. The deposited surfaces were incubated at 4 °C overnight in simple humidity chambers. Immediately prior to AFM assays, we repeatedly washed the coverslips by pipetting 1 mL of buffer over the sample (held at ~45 degrees) a minimum of 10 times. Care was taken to avoid dewetting the surface during rinsing. For the α_3D assay, we rinsed and performed the experiment in a buffer of 50 mM sodium phosphate (pH 7.0) and 150 mM NaCl. For the calmodulin assay, we first rinsed in 50 mM TrisHCl (pH 8.0) and 150 mM KCl and then rinsed with at least 3 mL of 50 mM TrisHCl (pH 8.0), 150 mM KCl, and 10 mM $CaCl_2$. The calmodulin AFM assays were performed in this calcium-containing buffer. Note, the initial rinsing in the absence of $CaCl_2$ avoids the known precipitation of phosphate buffers by $CaCl_2$ before introducing the $CaCl_2$ needed study the properly folded calcium-binding protein calmodulin.

Data-acquisition protocol for protein-unfolding assays. We used a multi-step process to measure the temporal resolution of the cantilever during a single-molecule assay. As illustrated in Fig. S6 A, we initially gently pressed the tip into the surface at ~150 pN for 1 s to promote attachment between the streptavidin-coated tip and the biotin-labeled polyprotein. We then retracted the tip from the surface at 400 nm/s until a force of 40 pN was reached at a tip-sample separation of at least ~80 nm (Fig. S6 B, red curve). This real-time triggering scheme selected for molecules attached to the cantilever while suppressing triggering on surface adhesion. Upon detection of a candidate molecule, we returned the cantilever to within 5 nm of the surface (*i.e, F* ≈ 0 pN) (Fig. S6 B, purple curve) and paused for 1 s to promote refolding. We next stretched the polyprotein to a predetermined extension based on the location of the first NuG2 unfolding event and only analyzed traces in which α_3D and three of the four NuG2 domains unfolded but the fourth NuG2 domain remained folded (Fig. S6 C). We then moved the cantilever to apply 80 pN across the polyprotein and then held the cantilever stationary (v = 0 nm/s) for 1 s during which the final NuG2 domain unfolded (Fig S6 D). Following this unfolding event, we lowered the tip again to within 5 nm of the surface for 1 s to promote refolding and then retracted the cantilever at v = 400 nm/s to unfold the entire polyprotein and detach it from the tip (Fig. S6 E). This final unfolding event ensured that the analyzed events arose from single polyproteins. We recorded the cantilever deflection at several different data-acquisition rates during this process. Specifically, we measured at 5 kHz during Fig. S6 B, while the second retraction and final retraction were recorded at 50 kHz (Fig. S6 C, E). To determine the cantilever response at high-time resolution, we concurrently sampled the second retraction and subsequent pause (Fig. S6 C, D) at 50 kHz and 500 kHz.

We used a simpler data-acquisition protocol for the calmodulin assay. As with α_3D assay, we first used a real-time trigger to select for a connection by retracting the cantilever at 400 nm/s until the F = 40 pN at a tip-sample separation of at least ~80 nm. Upon detection of a candidate

molecule, we again returned the cantilever to within 5 nm of the surface and paused for 1 s to promote refolding. We next retracted the tip at either 100 nm/s for the calmodulin-alone assay (Fig. 3 A, B) or 400 nm/s for calmodulin unfolding in the presence of myosin light chain kinase (Fig. 3 C). The initial retraction and refolding were digitized at 5 kHz, while the final retraction was recorded at 50 kHz. For samples containing the myosin light chain kinase peptide (GenScript, Calmodulin Binding Peptide 1, RP13247), it was introduced at 1 μM concentration.

DATA ANALYSIS

Protein data: The smoothing of each data set is noted in figure captions. For data recorded at 50 kHz, we applied a 2nd-order Savitsky-Galoy filter to the data. When an *n*-point smoothing filter is applied, we report the smoothed bandwidth as the original sampling frequency divided by *n*. For the high-bandwidth data recorded at 500 kHz, we applied a digital narrowband (300 Hz) notch filter at 125 kHz. This filter removes a known drive frequency in our AFM that occasionally contributes noise to the measurement. For the data smoothed to 5 kHz in Fig. S1, we applied a digital low-pass filter with a passband ending at 5 kHz.

Although the cantilever geometries preserved high laser reflectivity, small interference artifacts remained and needed to be computationally removed. We removed these optical-interference artifacts in a post-processing step, as described previously (3). Briefly, we used a heuristic model to describe the sine-wave-like interference artifact:

$$V_d = A_1 + A_2 \cdot Z_{\mathrm{PZT}} + (A_3 + A_4 \cdot Z_{\mathrm{PZT}}) \cdot \sin[A_5 + A_6 \cdot Z_{\mathrm{PZT}}]$$

Where V_{D} is the deflection voltage, Z_{PZT} is the Z-stage position sensor, and A_1, A_2, A_3, A_4, A_5, A_6 are fit parameters that are determined from the approach portion of the trace. This model then allows us to correct the retraction curves to eliminate the contribution from the interference artifact.

We analyzed the resulting force-extension curves (FECs) using an improved numerical approximation for an inextensible worm-like chain (WLC) model (13). FECs for a wide variety of biopolymers including DNA and proteins have been well described by a WLC model. The WLC model is parameterized by the persistence length (p) and contour length (L_0) of the polymer. In our fits, we used p = 0.4 nm, a common value for AFM-based SMFS. As each protein domain in the polyprotein unfolded, the contour length should increase by a fixed length (ΔL_0) proportional to the number of the released amino acids. As shown in Figure S7, the FECs measured with modified cantilevers were well described by WLC fits.

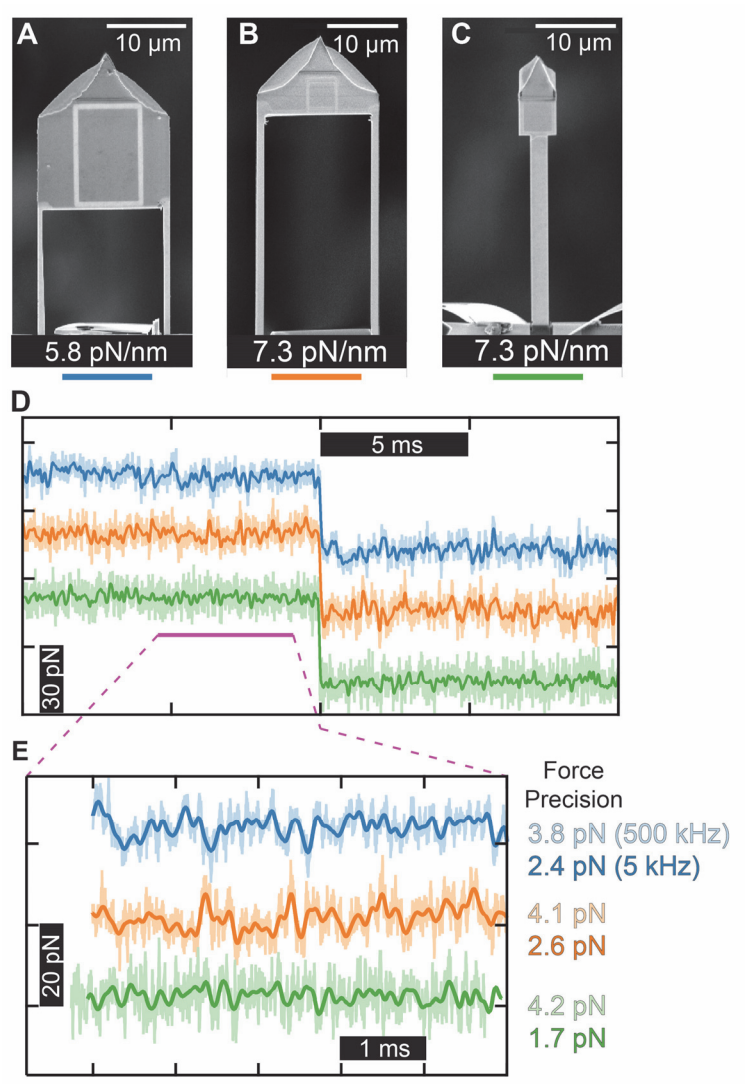

Figure S1: Improved force precision visualized in the time domain. (A-C) SEM image and *k* of the modified cantilevers shown in Fig. 1,2. Color below the image corresponds to the traces shown in panels (D) and (E). (D) High-bandwidth force-vs-time traces showing the unfolding of the fourth NuG2 domain at v = 0 nm/s. Data taken from Fig. 2 B. Filtering for the light and dark colored traces are 500 and 5 kHz, respectively. (E) Force-vs-time trace immediately before the rupture of the fourth NuG2 domain. The RMS force precision for each trace is shown to the right using the same smoothing as in panel (D).

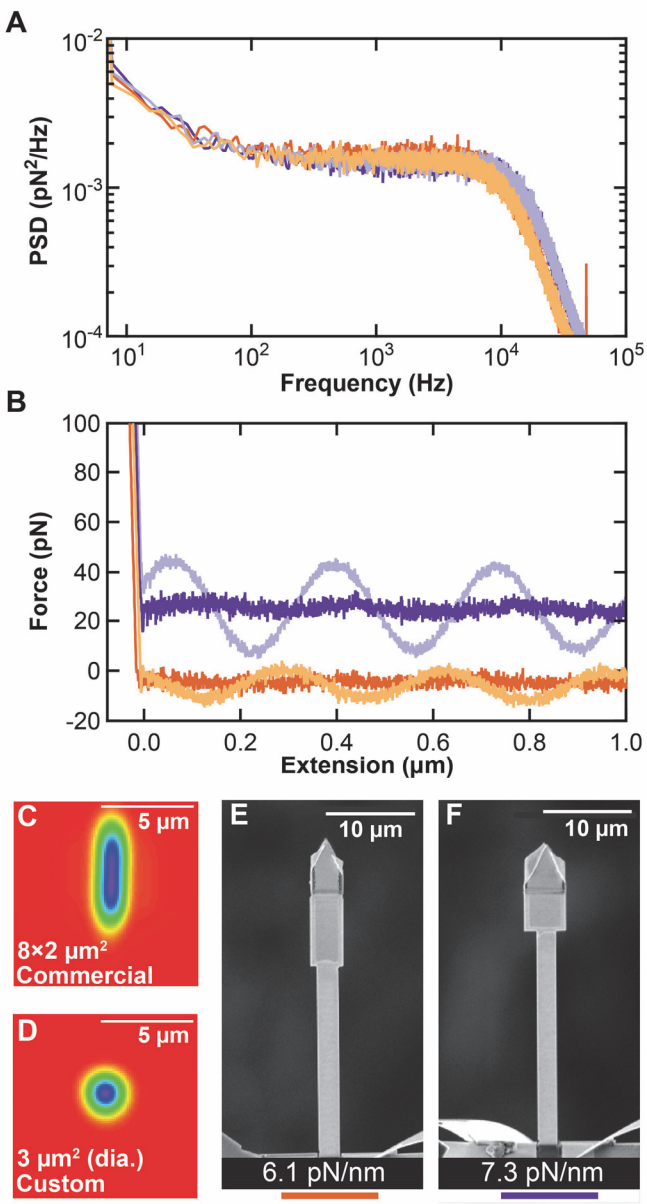

Figure S2: Detecting Warhammers with a commercial-detection module. (A) Force power spectral density (PSD) of the standard (purple) and extended Warhammer (orange). The darker color traces were taken using a custom detection module (3-μm-dia) while the lighter color traces were taken with the commercial small-spot-size module. The overlap of the PSDs shows no change in measured precision over all f between the different detection modules. (B) Force-extension traces show the optical-interference artifact for the standard (purple) and an extended (orange) Warhammer geometry. (C,D) Measured spatial distribution of the spot size formed by the commercial and custom detection modules. (E,F) SEM images (prior to gold etching) of an extended and normal Warhammer style cantilever showing the lengthened yet narrowed reflective patch (7.4×2.7 μm^2) for an extended Warhammer relative to a standard patch (4×4 μm^2). The extend geometry reduced the optical-interference artifact when using the commercial small-spot-size module as shown in panel B with minimal change in f_c (16 kHz vs 19 kHz, respectively).

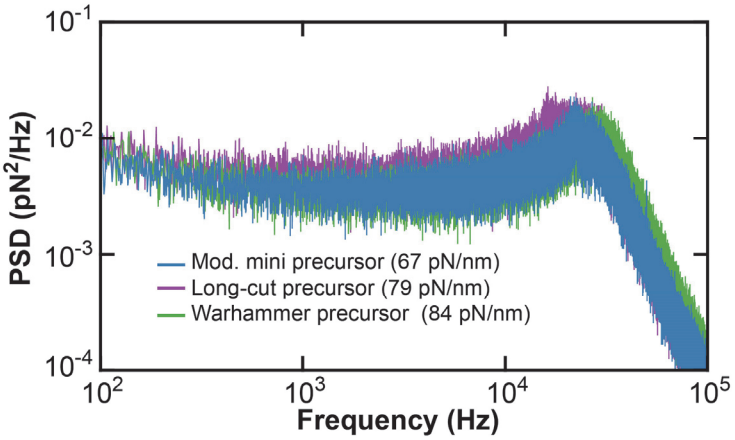

Figure S3: Mechanical properties of the compared cantilevers prior to modifications. Force power spectral density (PSD) in liquid plotted as a function of frequency for three modified BioLever Minis shown in Figure 1 and 2 prior to their modification. The *k* of each cantilever determined in air is listed. These three cantilevers were chosen for modification due to the similarity of their mechanical properties (*i.e*, *k, Q,* and PSD) to facilitate comparison.

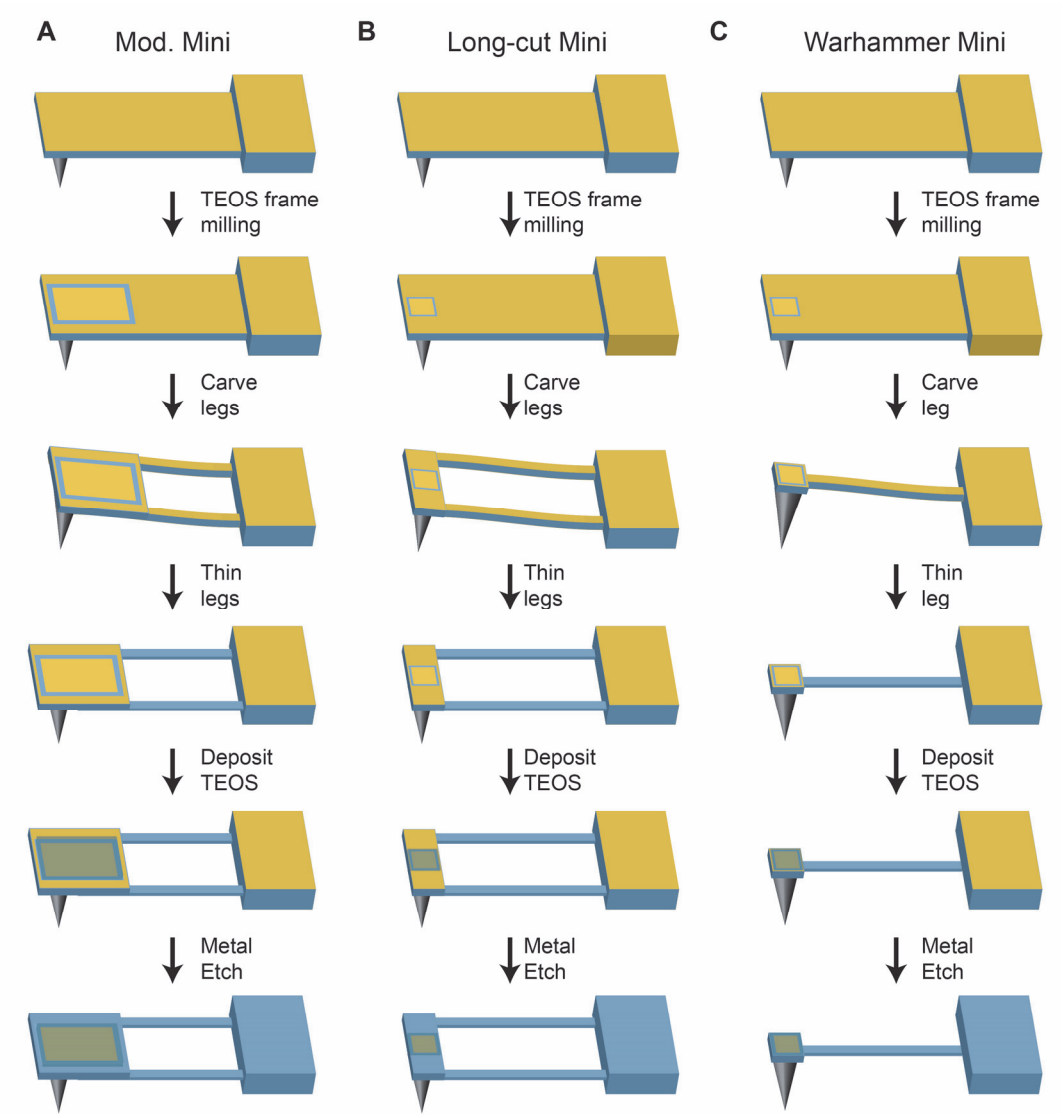

Figure S4: Cantilever modification protocol. A cartoon depiction of the process for focused-ion beam (FIB) modification of the three cantilever geometries investigated: (A) a Mod Mini, (B) a Long-cut Mini, and (C) a Warhammer. The general process for each cantilever geometry consisted of five processing steps: TEOS framing, carving out the legs, thinning the legs, depositing the TEOS, and a wet etch to remove the gold and underlying chromium layers.

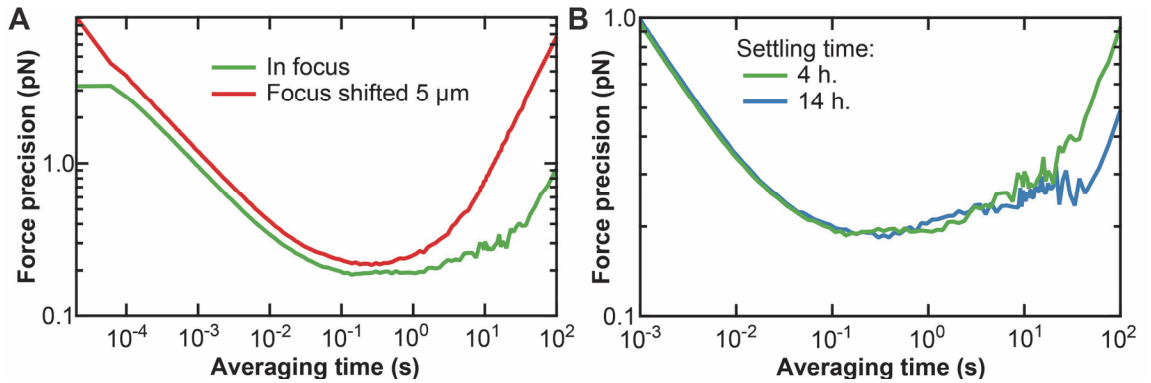

Figure S5: Improved long-term stability. (A) Variation in measured force precision over a given averaging time when changing the vertical position of the detector focus for a Warhammer in liquid positioned 50 nm over the surface. Specifically, measured long-term stability was significantly degraded (red) when the focus was shifted 5-µm vertically upward from the visible sharp focus. (B) Improvement in measured force precision over long periods when the cantilever was allowed to settle overnight versus 4 h (blue vs. green respectively).

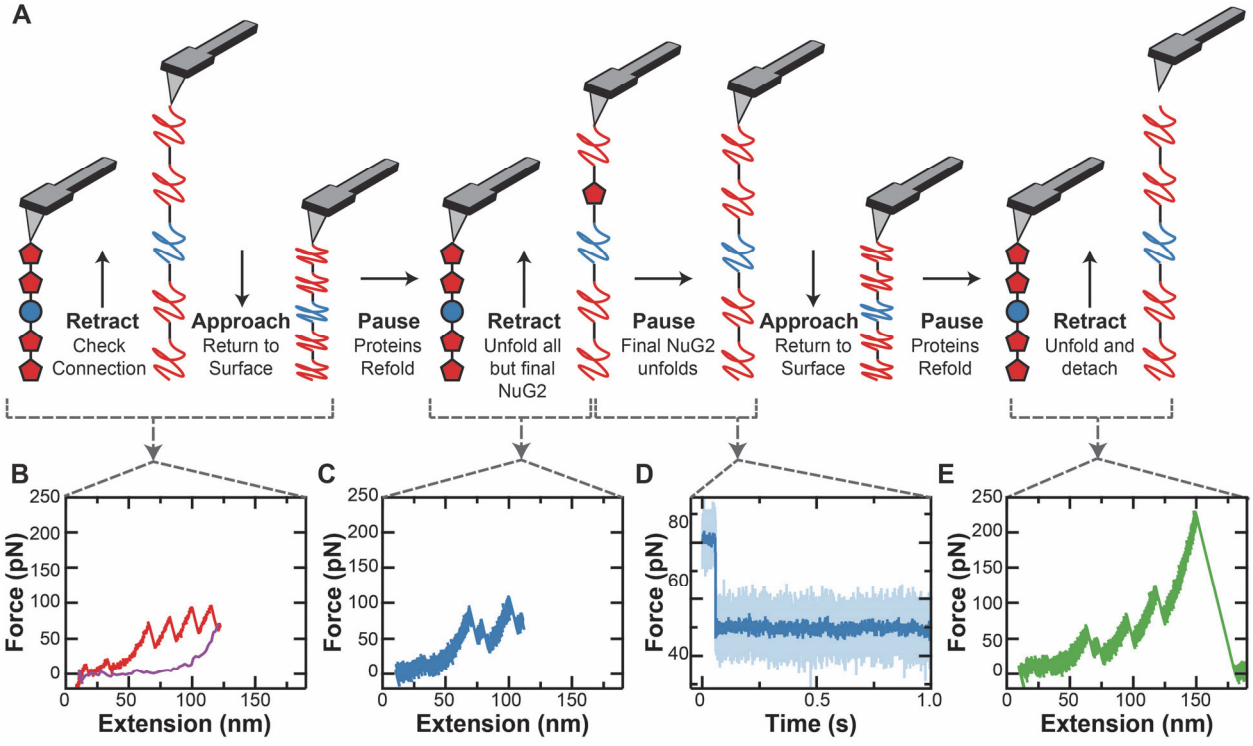

Figure S6: Multi-step unfolding protocol for measuring temporal response during a protein-unfolding assay. (A) A pictorial description of the unfolding protocol used to observe unfolding of a single NuG2 from a predetermined force. The four domains of NuG2 are depicted in red while the single domain of α_3D is shown in blue. Geometric shapes (pentagons and circles) represent folded domains while a linear depiction represents an unfolded domain. (B) Force-extension curve (FEC) shows the initial unfolding (red) of the polyprotein at v = 400 nm/s up to force (40 pN) and extension (>80 nm) values recognized by a real-time trigger scheme that selects for a promising candidate molecule. After triggering, the tip was then returned to the surface, resulting in a second FEC (purple). (C) FEC showing the stretching of the polyprotein to an extension leading to 80 pN of applied force and followed by the unfolding of the remaining single NuG2 domain. (D) Force-vs-time plot during a pause at constant stage position (v = 0 nm/s) (blue), during which the final NuG2 domain unfolded. (E) FEC showing the final unfolding curve after letting the polyprotein refold at $F \approx 0$ pN for 1 s. This final FEC shows all four NuG2 domains and the α_3D domain unfold, assuring a single polyprotein was measured. Data in panels B, C, and E filtered to 50 kHz. Data in panel D filtered to 50 kHz (light blue) and 1 kHz (dark blue).

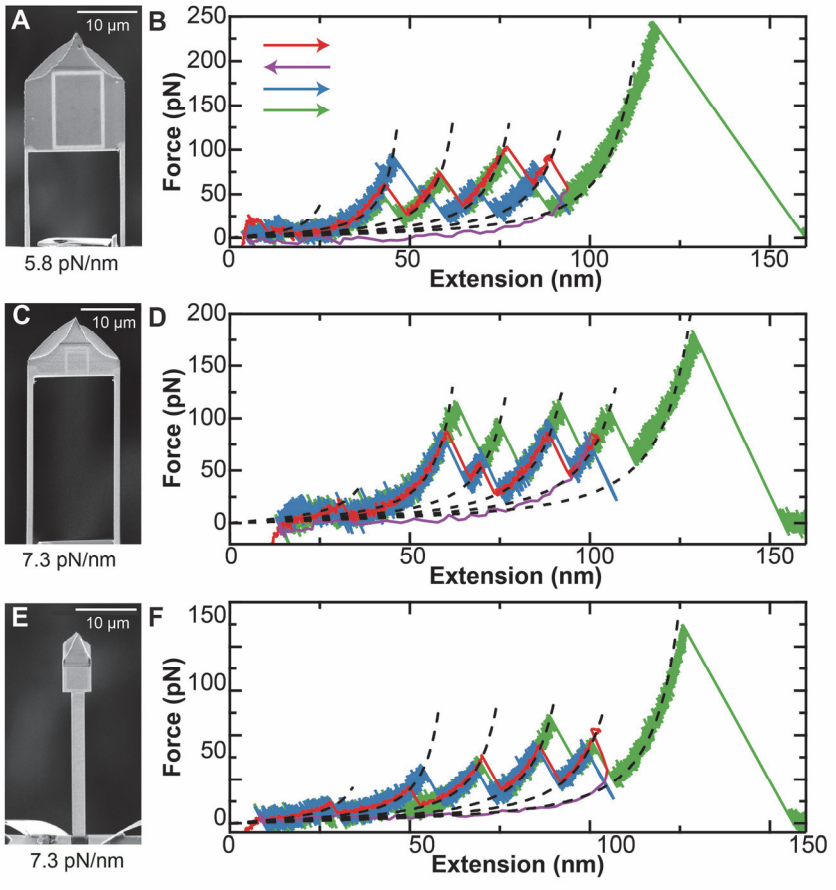

Figure S7: Protein-unfolding data well modeled by WLC fits. (A) An SEM image of a modified BioLever Mini, with its measured stiffness. (B) Force-extension curves acquired during the multi-step unfolding protocol (Fig. S6) used to determine the cantilever response for the cantilever shown in panel A. Red and purple traces represent the first unfolding and refolding step, respectively (Fig. S6 B). The blue trace shows the unfolding of α_3D and four domains of NuG2 (Fig. S6 C, D). The green trace shows the final unfolding record after allowing the protein to refold for 1 s at $F \approx 0$ pN. (C) An SEM image of a Long Cut Mini. (D) FEC acquired using the Long Cut Mini shown in panel C, with the same color coding as in B. (E) An SEM image of a Warhammer. (F) FEC acquired using the Warhammer shown in panel E with the same color coding as in B. Data in red and purple acquired at 5 kHz, data in blue and green acquired at 50 kHz.

REFERENCES

1. Faulk, J. K., D. T. Edwards, …, T. T. Perkins. 2017. Improved force spectroscopy using focused-ion-beam-modified cantilevers. *Methods Enzymol.* 582:321-351.
2. Bull, M. S., R. M. Sullan, …, T. T. Perkins. 2014. Improved single molecule force spectroscopy using micromachined cantilevers. *ACS Nano* 8:4984-4995.
3. Edwards, D. T., J. K. Faulk, …, T. T. Perkins. 2015. Optimizing 1-μs-resolution single-molecule force spectroscopy on a commercial atomic force microscope. *Nano Lett.* 15:7091-7098.
4. Rico, F., L. Gonzalez, …, S. Scheuring. 2013. High-speed force spectroscopy unfolds titin at the velocity of molecular dynamics simulations. *Science* 342:741-743.
5. Yu, H., M. G. Siewny, …, T. T. Perkins. 2017. Hidden dynamics in the unfolding of individual bacteriorhodopsin proteins. *Science* 355:945-950.
6. Proksch, R., T. E. Schaffer, …, M. B. Viani. 2004. Finite optical spot size and position corrections in thermal spring constant calibration. *Nanotechnology* 15:1344-1350.
7. Sullivan, D. B., D. W. Allan, …, E. L. Walls, editors. 1990. Characterization of Clocks and Oscillators. U.S. Government Printing Office, Washington.
8. Churnside, A. B., R. M. Sullan, …, T. T. Perkins. 2012. Routine and timely sub-picoNewton force stability and precision for biological applications of atomic force microscopy. *Nano Lett.* 12:3557-3561.
9. Walder, R., M.-A. LeBlanc, …, T. T. Perkins. 2017. Rapid characterization of a mechanically labile α-helical protein enabled by efficient site-specific bioconjugation. *J. Am. Chem. Soc.* 139:9867–9875.
10. Nauli, S., B. Kuhlman, and D. Baker. 2001. Computer-based redesign of a protein folding pathway. *Nat. Struct. Biol.* 8:602-605.
11. Cao, Y., M. M. Balamurali, …, H. B. Li. 2007. A functional single-molecule binding assay via force spectroscopy. *Proc. Natl. Acad. Sci. U.S.A.* 104:15677-15681.
12. He, C., C. Hu, …, H. Li. 2015. Direct observation of the reversible two-state unfolding and refolding of an alpha/beta protein by single-molecule atomic force microscopy. *Angew. Chem. Int. Edit.* 54:9921-9925.
13. Bouchiat, C., M. D. Wang, …, V. Croquette. 1999. Estimating the persistence length of a worm-like chain molecule from force-extension measurements. *Biophys. J.* 76:409-413.